Graphene Oxide/Fe_3O_4 Magnetic Nanocomposites for Efficient Recovery of Indium①

WANG Ling-Hang[a, b] QIU Zhi-Hua[b] CHI Li-Sheng[b②]

[a] (*College of Chemistry, Fuzhou University, Fuzhou* 350108, *China*)

[b] (*Fujian Province Joint Innovation Key Laboratory of Fuel and Materials in Clean Nuclear Energy System, Fujian Institute of Research on the Structure of Matter, Chinese Academy of Sciences, Fuzhou* 350108, *China*)

ABSTRACT Adsorbent has been widely used for the recovery and enrichment of rare metals from waste water. Herein, a graphene-based adsorbent, graphene oxide/Fe_3O_4 (GO/Fe_3O_4) nanocomposite, was prepared by a facile hydrothermal method, and characterized by X-ray diffraction, Scanning Electron Microscope, X-ray Photoelectron Spectroscopy, Zeta potential and magnetization. The material has been explored for the recovery of In from simulated waste water. The test results show that the nanocomposite has a reasonable adsorption capacity on indium in a wide pH range, e.g., the adsorption percent and quantity of In(Ⅲ) from the aqueous solutions at pH = 4 and C_0 = 50 mg·L^{-1} are 91% and 43.98 mg·L^{-1}, respectively. In addition, the nanocomposites maintain a 75.5% cycling capacity and a 71% removal efficiency after five continuous cycles due to their novel properties of high specific surface area and superparamagnetism. The pseudo-second-order adsorption model can be used to interpret the kinetic data. High adsorption efficiency and good reusability can make the nanocomposite a promising adsorbent for recovery of In(Ⅲ).

Keywords: adsorbent, graphene oxide, Fe_3O_4 magnetic nanoparticles (NPs), nanocomposites, In(Ⅲ);

DOI: 10.14102/j.cnki.0254-5861.2011-3161

1 INTRODUCTION

Metal indium is widely used in medical, defense, high-technology and energy industries due to its outstanding properties such as good ductility, strong plasticity, low melting point and low resistance. As indium is a low abundance element in earth and usually accompanied with other elements in minerals[1-3], selectively recovering indium from the aqueous solutions has become an important research topic in the world and has been proved to be an effective method for In enrichment. At present, the methods of recovering indium from wastewater include nanofiltration membrane[4], electro-analytical method[5], adsorption[6, 7] and supercritical CO_2 extraction[8]. However, these methods pose a challenge for complete recovery, simplified operation, cost-effectivity and secondary waste discharge. With the increase in environmental awareness, the development of an advanced technology for effective recovery of indium is needed.

The economy and effectiveness of adsorption enrichment methods have regained attention in recent years as a number of new reusable adsorption materials with large adsorption capacity and high removal efficiency were discovered[9, 10]. Traditional adsorption materials such as activated carbon, zeolites and resins are readily available and inexpensive. However, these materials have several shortcomings such as small adsorption capacity, long adsorption time, low recovery and separation efficiency, and serious degradation. Recently, nanomaterials are found to have numerous advantages over conventional materials, e.g., magnetic nanoparticles (NPs) have high specific surface area, large surface-to-volume ratio, big adsorption capacity, and superparamagnetism. These materials would exhibit higher adsorption capacity when they are decorated onto graphene oxide (GO) sheets[11, 12] due to GO having high specific surface area, excellent thermal conductivity, electrical conductivity and mechanical properties[13, 14]. As GO is a derivative of graphene and contains a large number of functional groups, some substances can be attached onto the GO surfaces by bonding

Received 26 February 2021; accepted 24 March 2021

① This work is supported by the FJIRSM&IUE Joint Research Fund (No. RHZX-2018-006)

② Corresponding author. lchi@fjirsm.ac.cn

to the functional groups[15-17], such as GO with excellent adsorption effect on polycyclic aromatic hydrocarbons(PAHs) through π interaction and hydrophobic interaction[18]. As a result, the maximum adsorption amount of Cr(VI) from the solution at pH 3~4 and the initial concentration of 600 mg L^{-1} by the GO/Fe_3O_4 composites at the dose of 125 mg L^{-1} is 280.6 mg/g[19]. The adsorption of Hg(II) onto GO/Fe_3O_4 reached equilibrium within 4 minutes, and the adsorption capacity and adsorption percentage in the solution at pH 5, the initial Hg concentration of 300 mg L^{-1} and the adsorbent dose of 500 mg L^{-1} were 547.01 mg g^{-1} and 91.17%, respectively[20]. GO/Fe_3O_4 nanocomposites are considered as promising adsorbent materials because of their excellent magnetic properties, low toxicity, low cost and environmental friendliness[21, 22].

In this study, the GO/Fe_3O_4 nanocomposites were prepared by a facile hydrothermal method. With the aid of -COOH groups, Fe_3O_4 nanoparticles are chemically bonded to the GO sheet. The adsorption test results show that the GO/Fe_3O_4 nanocomposites have high efficiency and recyclability in removing In(Ⅲ) from the aqueous solution. The adsorption percent and amount of In from the solution at pH 4 and the initial In concentration of 50 mg L^{-1} are 91% and 43.98 mg L^{-1}, respectively. After five consecutive cycles, the remaining adsorption capacity of the material was 75.5% of the initial capacity.

2 EXPERIMENTAL

2. 1 Chemicals and materials

The chemicals used in the study include ferric chloride hexahydrate ($FeCl_3$ $6H_2O$) with 99% purity and N.N-dimethylformamide (DMF) with 99% purity, both of which were purchased from China National Medicines Co. Ltd, China. Graphene oxide with 95% purity which was purchased from Kaina Carbon New Materials, China, was prepared using the modified Hummers method.

2. 2 Preparation of GO/Fe_3O_4 nanoparticle composites

Synthesis of GO/Fe_3O_4 composite follows the procedure below. First weigh 0.1 g GO and load it into a 100 mL beaker, followed by adding 60 mL DMF and 15 mL ethylene glycol in the order. Ultrasonically disperse the solution for 2 h to make uniform GO. Then add 1.08 g $FeCl_3$ $6H_2O$ to the above mixed solution and ultrasonically disperse again for 2 hours, followed by adding 0.72 g urea, stirring for 30 minutes, and transferring to a stainless-steel reactor with tetrafluoroethylene lining for polymerization. Heat the reactor to 200 ℃ and maintain at the temperature for 12 h. After the reactor was cooled to room temperature, the product was magnetically separated, washed with anhydrous ethanol and water for 3~5 times, and then dried in a vacuum drying oven at 60 ℃ for 12 hours. The black powder composite material was obtained.

2. 3 Batch adsorption experiments

The adsorbent GO/Fe_3O_4 of 10 mg was weighed and added to 10 mL In solution in the form of In $(NO_3)_3$), which was loaded into a 10 mL PTFE centrifuge tube. The tube was shaken on a shaker at 250 rpm and room temperature for 24 hours to reach complete adsorption equilibrium. After adsorption, NaOH and HNO_3 were added to adjust pH of the solution to the desired value. Changes in their volumes are negligible. Place a magnet on the outer surface of the container to separate the adsorbent from the solution, take the supernatant out and filter the remaining solution with a water filter membrane with 0.22 μm.

The amount of adsorbed In was obtained by calculating the difference between the initial concentration (C_0) and equilibrium concentration (C_e) after reaching the adsorption equilibrium. The following equations are used to determine the percentage of adsorption (Eq. 1) and adsorption capacity (Eq. 2).

$$A(\%) = \frac{(C_0 - C_e)}{C_0} \times 100\% \quad (1)$$

$$q_e = \frac{V \times (C_0 - C_e)}{m} \quad (2)$$

where V is the volume of the solution and m is the mass of the adsorbent.

2. 4 Characterization methods

The indium concentrations of the obtained samples were measured using atomic absorption spectroscopy with ContrAA700 instrument made by Analytik Jena AG, Germany. X-ray diffraction (XRD) was used for identifying the phase of the samples. XRD pattern was collected on a Rigaku Miniflex600 with Cu$K\alpha$ radiation at λ = 1.5406 Å and scanning speed and step size at 5 ℃/min and 0.02°, respectively. Raman spectrum was measured on the LabRAM HR system made by HORIBA Scientific. The X-ray Photoelectron Spectroscopy (XPS) was conducted on a Thermo Fisher ESCALAB 250Xi spectrometer to study the oxidation state of iron. Scanning Electron Microscope (SEM) with Hitachi S4800 was used for studying the microstructures of samples. Fourier Transform Infrared Spectroscopy (FTIR) spectra were recorded on a Vertex70 infrared spectrometer to

obtain the structure information of GO/Fe_3O_4. The magnetic properties of GO/Fe_3O_4 were measured on a magnetic property measurement system (MPMS) with a superconducting quantum interference device (SQUID) magnetometer. Zeta potentials were collected on a BI-200SM Laser Particle Size and Zeta Potential Analyzer to study the stability of the solution.

3 RESULTS AND DISCUSSION

3. 1 Characterization of GO/Fe_3O_4

Fig. 1 displays the XRD patterns of GO/Fe_3O_4 and Fe_3O_4, both of which match well. The diffraction peaks located at 21.5 °, 29.8 °, 36.3 °, 42.8 °, 54.1 °, 58.1 ° and 61.7 ° can be assigned to (111), (220), (311), (400), (422), (511) and (440) reflections of the hexagonal Fe_3O_4 phase, respectively, based on PDF card 26-1136 of the standard XRD data. This indicates the presence of Fe_3O_4 in GO/Fe_3O_4. There is no clear graphene peak in the XRD pattern, suggesting that GO in GO/Fe_3O_4 may exist in the amorphous form.

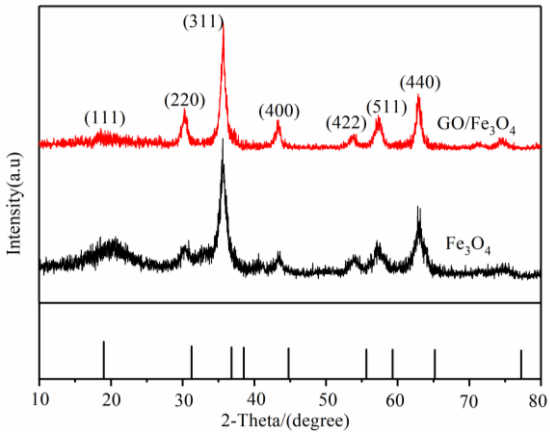

Fig. 1. XRD pattern of GO/Fe_3O_4

Fig. 2A and 2B displays SEM images of magnetic Fe_3O_4 and GO/Fe_3O_4 nanocomposites, respectively. Fe_3O_4 nanoparticles are relatively uniform and about 90 nm in size whereas in the GO/Fe_3O_4 nanocomposites, Fe_3O_4 nanoparticles are well distributed in the transparent GO film and reduced to about 20 nm in size. This suggests that GO/Fe_3O_4 nanocomposites reduce agglomeration of Fe_3O_4 nanoparticles.

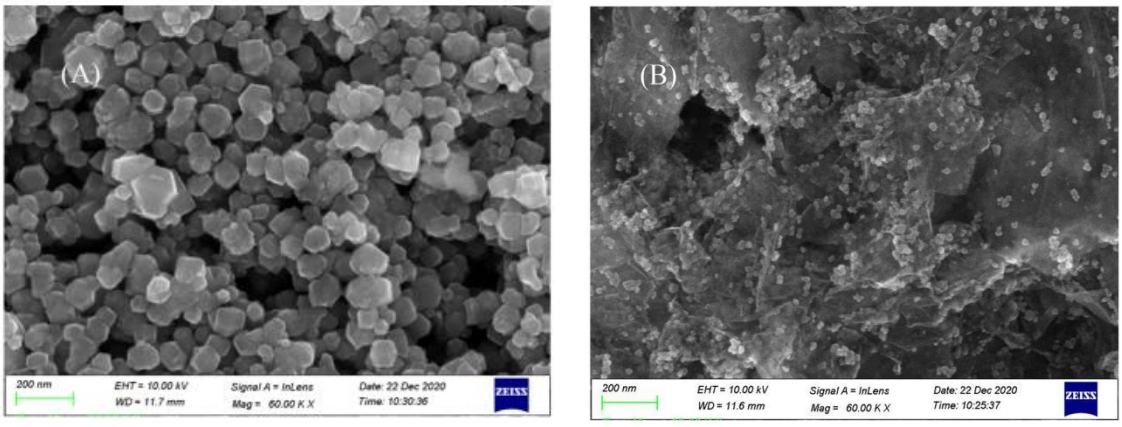

Fig. 2. (A) SEM images of Fe_3O_4, (B) SEM images of GO/Fe_3O_4

The chemical states of the elements in GO/Fe_3O_4 are studied by the XPS technique. Fig. 3A shows the full XPS spectrum of GO/Fe_3O_4 samples, in which the binding energies at 285, 530 and 712 eV are attributed to the presence of C1*s*, O1*s*, and Fe2*p*, respectively. This confirms the formation of GO/Fe_3O_4. The C1*s* peak can be deconvoluted into C−C, C−O,

O−C=O bonds in graphene oxide plane, whereas the O1s peaks at 530.12 and 533.7 eV result from the C−O and C−O bonds, respectively[27]. Fig. 3B shows a high resolution XPS spectrum of Fe2*p*, in which the peaks at 712.46 and 726.42 eV arise from Fe2$p_{3/2}$ and Fe2$p_{1/2}$, respectively. This is in agreement with the XPS of Fe_3O_4, indicative of the formation of Fe_3O_4 in the nanocomposites[23].

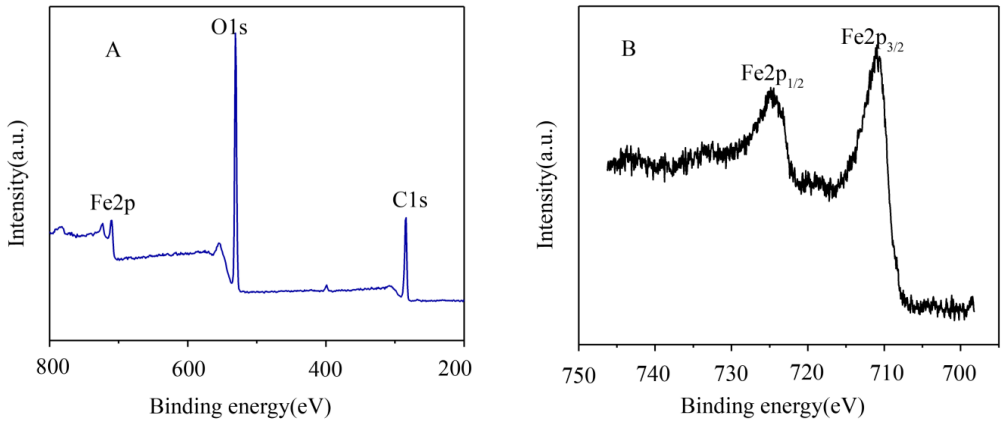

Fig. 3. (A) Full XPS spectrum, (B) XPS spectrum of Fe2*p*

Zeta potential is widely used to characterize the surface charge of an adsorbent as it reflects the stability of the sample in water[24]. The greater the absolute Zeta potential, the more stable the system and the less likely the material is to agglomerate in solution[25, 26]. The Zeta potential of GO/Fe_3O_4 was measured at pH = 4 to be 13.04, while the Zeta potential of Fe_3O_4 was –4.8. Under the same conditions, the absolute value of Zeta potential of GO/Fe_3O_4 is greater than that of Fe_3O_4, indicating better dispersion of GO/Fe_3O_4 in the solution.

The hysteresis loops of GO/Fe_3O_4 and Fe_3O_4 nanocomposites are shown in Fig. 4A, indicating they are superparamagnetic[27]. The saturation magnetization (Ms) of GO/Fe_3O_4 and Fe_3O_4 is 30.05 and 61.2 emu/g, respectively. Although the Ms of the GO/Fe_3O_4 nanocomposite is about 50% that of Fe_3O_4, it is promising as a magnetic adsorbent for removal of pollutants from the aqueous solutions or recycling of precious metals from the wastes.

Fig. 4B (left) shows that the GO/Fe_3O_4 nanoparticles can be uniformly dispersed in water to form stable suspensions due to high Zeta potential. Upon applying an external magnetic field to the suspension by a magnet, GO/Fe_3O_4 nanoparticles are rapidly attracted to the bottle wall, and the rest solution is almost clear, as shown in Fig. 4B (right). Therefore, the GO/Fe_3O_4 nanocomposite exhibits high dispersion and characteristics of magnetic separation. This kind of adsorbent material that can be rapidly separated by a magnet would be beneficial to the future adsorption application. It could not only reduce the cost of heavy metal treatment in aqueous solution, but also prevent the secondary waste pollution caused by adsorbent material.

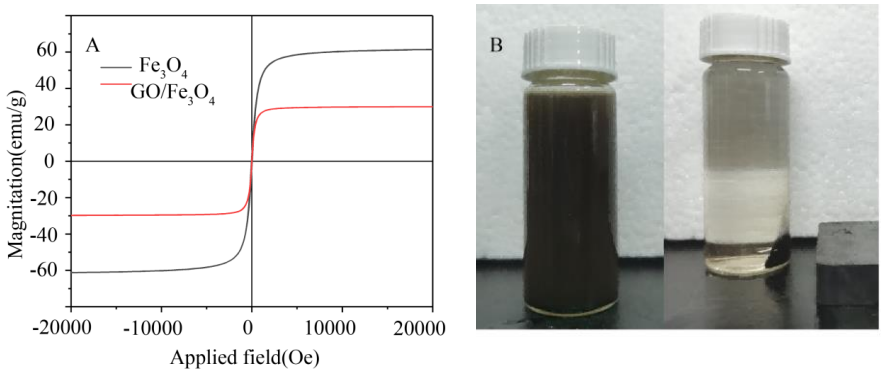

Fig. 4. (A) Magnetization hysteresis curves of GO/Fe_3O_4 and Fe_3O_4. (B) Magnet separation of GO/Fe_3O_4 nanoparticles

The Raman spectra of GO/Fe_3O_4 and Fe_3O_4 are displayed in Fig. 5A. Raman spectrum of GO/Fe_3O_4 has two striking peaks D and G located at 1346 and 1621.5 cm^{-1}, respectively[28], which are related to the disordered structure of graphene oxide and the extension of carbon-carbon bonds in the sp^2 plane. The strength ratio (I_D/I_G) of peaks D and G can be used to identify defects[29, 30]. In the case of GO/Fe_3O_4 nanocomposites, due to SERS effect[31], attachment of Fe_3O_4 nanoparticles onto the graphene oxide surface results in the enhanced Raman peaks D and G.

The infrared spectra of Fe_3O_4 and GO/Fe_3O_4 are displayed in Fig. 5B. In the GO/Fe_3O_4 FTIR spectrum, the peaks at 3445 and 1666 cm^{-1} correspond to the stretching vibration of O−H and C=C bonds, respectively, whereas those at 1480 and 1124 cm^{-1} are associated with the stretching vibration mode of C−OH and C−O[20]. These infrared peaks indicate the presence of hydrophilic functional groups, including O−H, C=O, C−O *etc*, on the surface or edge of GO, which will not only assist in maintaining the GO/Fe_3O_4 composite stable in the water system, but also interacting with the ions to be adsorbed. This is conducive to the enrichment of the adsorbates[32]. In addition, the peak at 590 cm^{-1} in Fig. 5B is associated with the stretching vibration of Fe−O in Fe_3O_4 nanoparticles[33]. The weak peaks at 3551 and 1670 cm^{-1} are likely associated with the stretching and bending vibration peaks of O−H due to Fe_3O_4 being prepared by hydrothermal method, which are consistent with the literature[34]. The infrared spectrum reveals that the compound contains two components, Fe_3O_4 and GO, indicating that the GO/Fe_3O_4 composite has been successfully synthesized.

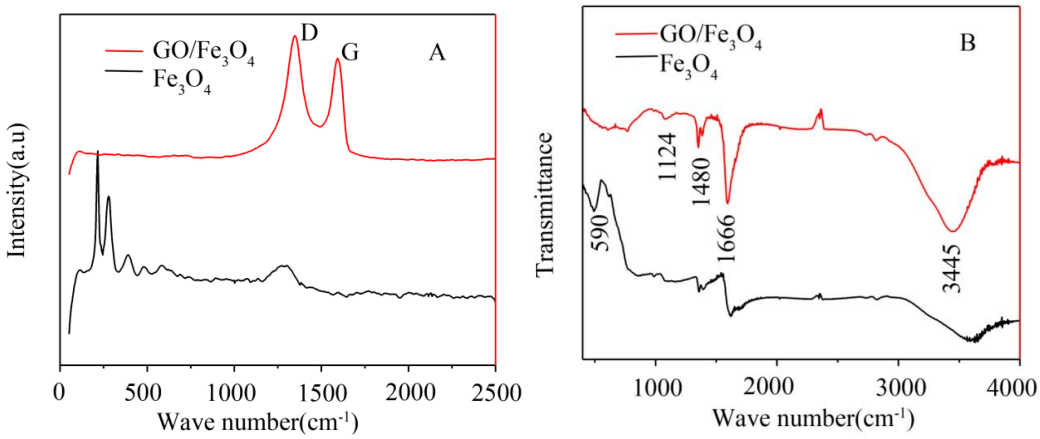

Fig. 5. (A) Raman spectra and (B) FTIR spectra of Fe_3O_4 and GO/Fe_3O_4

3. 2 Effect of contact time

The amount of adsorbed In as a function of contact time was studied and is plotted in Fig. 6. The adsorption of In on the GO/Fe_3O_4 sharply increased in the first 30 minutes, followed by reaching an asymptotic value with increasing the contact time. Later on, the vibration time of 24 h in all adsorption experiments was used to make sure that the adsorption equilibrium is completely established.

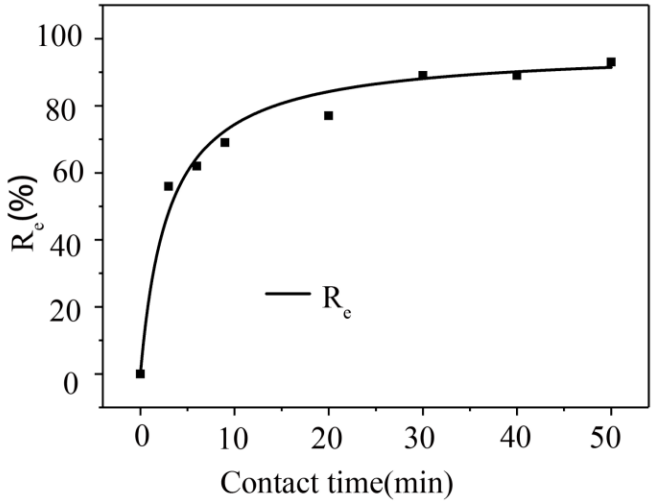

Fig. 6. Effect of contact time on the In adsorption at pH = 4, C_0 = 50 mg L^{-1} and T = 25 ℃

These adsorption kinetic data are explored to fit the pseudo-first- and pseudo-second-order models, which are expressed in Eqs. 3 and 4, respectively.

$$\log(q_e - q_t) = \log q_e - \frac{k_1}{2.303} t \quad (3)$$

$$\frac{t}{q_t} = \frac{1}{k_2 q_e^2} + \frac{t}{q_e} \quad (4)$$

where k_1 and k_2 are the pseudo-first-order and pseudo-second-order rate constants, respectively, q_e is the capacity of In adsorbed at equilibrium (mg Ł$^{-1}$), and q_t is the In mass (mg Ł$^{-1}$) adsorbed on the adsorbent surface at t time[33, 34].

Fitting of adsorption kinetic data with the pseudo-first- and pseudo-second-order models was performed and shown in Fig. 7. The fitting parameters are summarized in Table 1. These fitting parameters show that the adsorption data fit to the pseudo-second-order model better than the pseudo-first-order kinetic model as $R^2 > 0.998$. For the pseudo-second-order model, chemisorption which proceeds with valence forces through sharing electron or exchange is a rate-controlling step[35], which will be briefly discussed in Section 3.3.

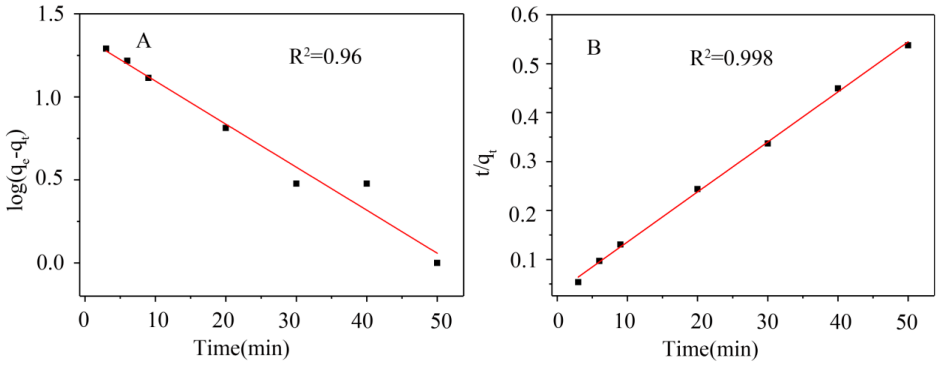

Fig. 7. Kinetic model of In adsorption: (A) pseudo-first-order kinetics, (B) pseudo-second-order kinetics

Table 1. Kinetic Sorption Constant Parameters of In(Ⅲ)

Metal ions	Pseudo-first-order			Pseudo-second-order		
	q_e(mg g^{-1})	k_1(min^{-1})	R^2	q_e(mg g^{-1})	k_2(g mg^{-1} min^{-1})	R^2
In(Ⅲ)	47.5	–0.02591	0.96467	47.5	0.01022	0.99834

3. 3 Effect of pH

To study the effect of pH on the adsorption of In onto GO/Fe_3O_4 nanocomposites, the $In(NO_3)_3$ aqueous solution at In concentration of 50 mg Ł$^{-1}$ and the initial pH of 4 was prepared. pH of the solution was adjusted from 2 to 12 with HNO_3 and NaOH. Fig. 8 shows that the adsorption of In onto the GO/Fe_3O_4 increases significantly from 7% to 99.5% with increasing pH from 2.0 to 6.0, followed by a platform in the range of 6~8. As pH continues to rise, adsorption efficiency decreases and then approaches to another platform.

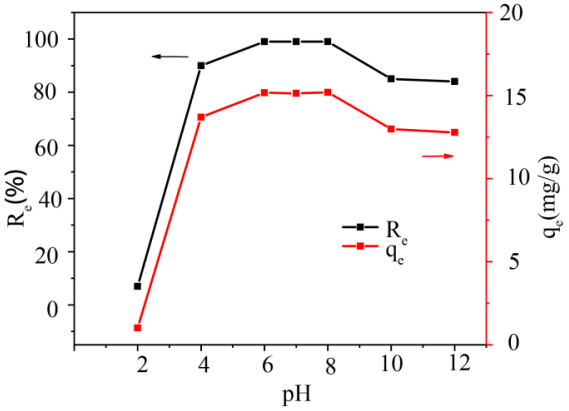

Fig. 8. Effect of solution pH on the In(Ⅲ) adsorption at pH = 2-12, C_0 = 50 mg Ł$^{-1}$, t = 24 h and T = 25 ℃

In(III) species in aqueous solution could exist in the form of In^{3+}, $In(OH)^{2+}$, $In(OH)_2^+$, $In(OH)_3$ and $In(OH)_4^-$, depending on pH. At pH < 6, In(III) is mainly in the form of In^{3+}. Therefore, In(Ⅲ) is removed mainly through adsorption process. At pH < pH_{zpc}, protonation of the GO/Fe_3O_4 nanocomposite results in the surfaces being positively charged[27]. The electrostatic repulsion between positive charges of In^{3+} and the GO/Fe_3O_4 surface leads to low adsorption in this pH range. At pH > pH_{zpc}, as carboxyl functional groups on GO surface dissociate, the concentration of deprotonated sites increases with increasing the pH value. The deprotonated site is easier to attract metal ions by electrostatic interaction, which is conducive to form complexes between In^{3+}, $In(OH)^{2+}$, $In(OH)_2^+$ and GO/Fe_3O_4. Thus, the adsorption of In at pH 2~6 increases sharply. When pH is greater than 6.0 , indium ions get precipitated due to the formation of indium hydroxide, which is dissolved to form $In(OH)_4^-$ when pH is greater than 10[36]. This indicates that at higher pH, In(Ⅲ) removal is mainly achieved by precipitation.

As the competitive adsorption of H ions with indium ions onto GO/Fe_3O_4 occurs at lower pH and indium precipitates form at higher pH, the optimum pH at which maximum adsorption of In onto GO/Fe_3O_4 occurs is about 4.

3. 4 Effect of adsorbent content

The effect of adsorbent content on the amount of In adsorbed onto GO/Fe_3O_4 was studied to optimize the adsorption efficiency and evaluate the availability of an adsorbent. The test results are presented in Fig. 9. It is seen that with increase in the adsorbent content, the adsorption amount of In increases gradually, while the q_e value of the adsorbent quickly rises to reach the highest at the adsorbent concentration of 1 g Ł$^{-1}$, followed by decreasing gradually. The number of adsorption sites increases with increasing the adsorbent concentration, thus resulting in increase in adsorption percent. However, with further increasing the adsorbent concentration, part of adsorption sites may become unavailable due to agglomeration, leading to decrease in the adsorption amount.

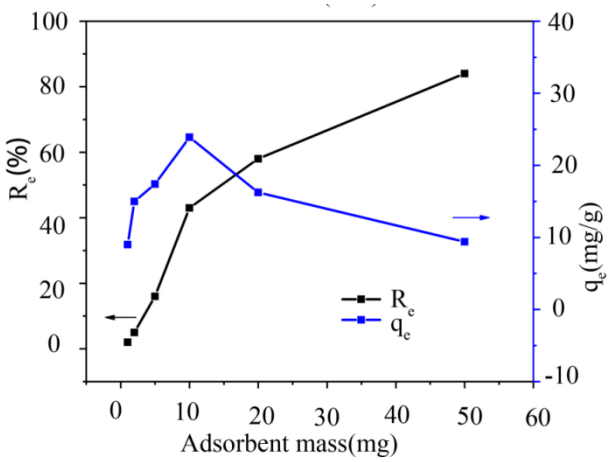

Fig. 9. Effect of adsorbent content on the In(Ⅲ) adsorption at pH 4 and the initial concentration of 50 mg Ł$^{-1}$

3. 5 Effect of In concentration

The adsorption efficiency of GO/Fe_3O_4 in the In solution at the initial concentration of 5~125 mg Ł$^{-1}$ is investigated to evaluate the adaptability of GO/Fe_3O_4 to the In concentration. Fig. 10 shows that the adsorption percent decreases with increasing the In concentration. For an adsorbent, higher concentration of the solution will produce higher concentration gradient at interface between solution and adsorbent, which facilitates the adsorbate to transport to the adsorbent. At low In concentration, In ions may be adsorbed onto GO/Fe_3O_4 nanocomposites without competition, leading to the high adsorption efficiency. As shown in Fig. 10, the highest adsorption percent of the GO/Fe_3O_4 nanocomposite at the initial concentration of 25 mg Ł$^{-1}$ is 97.2%. With increase in indium concentration, more In ions compete on the limited adsorption sites, thus leading to the decrease in the adsorption efficiency. Furthermore, when the adsorption sites are occupied gradually, more In ions compete on fewer adsorption sites, causing more significant decrease in the adsorption percent, as seen in Fig. 10, when the initial In concentration is greater than 110 mg/L[37].

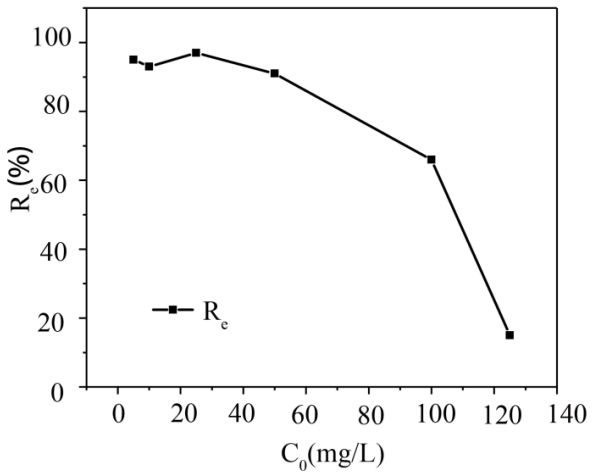

Fig. 10. Effect of indium ion concentration on the In(Ⅲ) adsorption (pH = 4, t = 24 h and T = 25 ℃). GO/Fe_3O_4 dosage is 1 g Ł$^{-1}$

3. 6 Recycling performance of GO/Fe_3O_4

Recycling of the GO/Fe_3O_4 nanocomposites for recovery of In(Ⅲ) from the aqueous solution is shown in Fig. 11. Desorption was performed with a HNO_3 concentration of 0.01 mol Ł$^{-1}$. After four and five adsorption-desorption cycles, the removal efficiency maintained at about 91% and 71%, respectively. The maximum adsorption quantity of is 43.98 mg Ł$^{-1}$ with the recovery efficiency of 75.5%. The excellent recycling performance indicates that the GO/Fe_3O_4 nanocomposite is reusable and an economic adsorbent for recovery of In(Ⅲ) from the aqueous solution. In addition, the adsorbent can be well dispersed in water, which is conducive to remove the pollutants from the aqueous solutions. Therefore, the GO/Fe_3O_4 nanocomposite is not only a recyclable adsorbent, but also easy to handle.

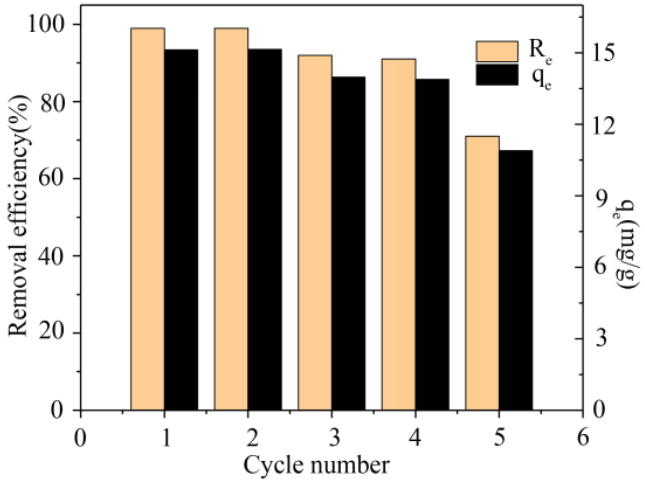

Fig. 11. Recycling of GO/Fe_3O_4 for In(Ⅲ) removal at pH = 4, C0 = 20 mg Ł$^{-1}$ and T = 293 K

4 CONCLUSION

In this study, magnetic nanocomposite GO/Fe_3O_4 was prepared by a facile hydrothermal method and has been used for the recovery of In(Ⅲ) from the simulated waste. The adsorption percent and quantity of In(Ⅲ) in the solution at pH = 4 and C_0 = 50 mg Ł$^{-1}$ are 91% and 43.98 mg Ł$^{-1}$, respectively. In addition, GO/Fe_3O_4 can be easily recycled by magnetic separation, and maintains a 75.5% cycle capacity after five continuous cycles. Both GO and Fe_3O_4 uptake In(Ⅲ) via donating electrons in oxygen atoms toward In(Ⅲ). High adsorption efficiency, easy recycling and good reusability can make GO/Fe_3O_4 be a promising adsorbent for the recovery of indium from the aqueous waste.

AUTHOR STATEMENT

L. S Chi planned and supervised the study. L. H Wang conducted experiments and analyzed the results with Z. H Qiu. L. H Wang prepared the manuscript after consulting with all authors.

DECLARATION OF COMPETING INTEREST

The authors declare that they have no known competing financial interests or personal relationships that may affect the work reported in this paper.

REFERENCES

(1) Calagui, M. J. C.; Senoro, D. B.; Kan, C.; Salvacion, J. W. L.; Futalan, C. M.; Wan, M. Adsorption of indium(III) ions from aqueous solution using chitosan-coated bentonite beads. *J. Hazard Mater.* **2014**, 277, 120–126.

(2) Minamisawa, H.; Murashima, K.; Minamisawa, M.; Arai, T.; Okutani, T. Determination of indium by graphite furnace atomic absorption spectrometry after coprecipitation with chitosan. *Anal. Sci*. **2003**, 19, 401–404.

(3) Liu, J. S.; Chen, H.; Chen, X. Y.; Guo, Z. L.; Hu, Y. C.; Liu, C. P.; Sun, Y. Z. Extraction and separation of In(III), Ga(III) and Zn(II) from sulfate solution using extraction resin. *Hydrometallurgy* **2006**, 82, 137–143.

(4) Wu, M.; Sun, D. D.; Tay, J. H. Effect of operating variables on rejection of indium using nanofiltration membranes. *J. Membr. Sci.* **2004**, 240, 105–111.

(5) Medvecky, L.; Briancin, J. Possibilities of simultaneous determination of indium and gallium in binary InGa alloys by anodic stripping voltammetry in acetate buffer. *Chem. Pap*. **2004**, 58, 93–100.

(6) Takashi, O.; Tamaoki, K.; Saitoh, N.; Saitoh, N.; Higashi, A.; Konish, Y. Recovery of indium from aqueous solutions by the Gram-negative bacterium Shewanella algae. *Biochem. Eng. J*. **2012**, 63, 129–133.

(7) Hu, J.; Chen, G. H.; Lo, I. M. C. Removal and recovery of Cr(VI) from wastewater by maghemite nanoparticles. *Water Res*. **2005**, 39, 4528–4536.

(8) Chou, W. L.; Yang, K. C. Effect of various chelating agents on supercritical carbon dioxide extraction of indium(III) ions from acidic aqueous solution. *J. Hazard. Mater.* **2008**, 154, 498–505.

(9) Zhao, D. L.; Gao, X.; Wu, C. N.; Xie, R.; Feng, S. J.; Chen, C. L. Facile preparation of amino functionalized graphene oxide decorated with Fe_3O_4 nanoparticles for the adsorption of Cr(VI). *Appl. Surf. Sci.* **2016**, 384, 1–9.

(10) Ahn, C. K.; Park, D.; Woo, S. H.; Park, J. M. Removal of cationic heavy metal from aqueous solution by activated carbon impregnated with anionic surfactants. *J. Hazard. Mater.* **2009**, 164, 1130–1136.

(11) Fu, Y.; Wang, J. Y.; Liu, Q. X.; Zeng, H. B. Water-dispersible magnetic nanoparticle-graphene oxide composites for selenium removal. *Carbon* **2014**, 77, 710–721.

(12) Yao, Y. J.; Miao, S. D.; Liu, S. Z.; Ma, L. P.; Sun, H. Q.; Wang, S. B. Synthesis, characterization, and adsorption properties of magnetic Fe_3O_4@graphene nanocomposite. *Chem. Eng. J*. **2012**, 184, 326–332.

(13) Allen, M. J.; Tung, V. C.; Kaner, R. B. Honeycomb carbon: a review of graphene. *Chem. Rev.* **2009**, 110, 132–145.

(14) Ates, M.; Bayrak, Y.; Yoruk, O.; Caliskan, S. Reduced graphene oxide/titanium oxide nanocomposite synthesis via microwave-assisted method and supercapacitor behaviors. *J. Alloy. Compd*. **2017**, 728, 541–551.

(15) Yang, X. Y.; Zhang, X. Y.; Ma, Y. F.; Huang, Y.; Wang, Y. S.; Chen, Y. S. Superparamagnetic graphene oxide-Fe_3O_4 nanoparticles hybrid for controlled targeted drug carriers. *J. Mater. Chem.* **2009**, 19, 2710–2714.

(16) Goncalves, G.; Marques, P. A. A. P.; Granadeiro, C. M.; Granadeiro, C. M.; Nogueira, H. I. S.; Singh, M. K.; Gracio, J. Surface modification of graphene nanosheets with gold nanoparticles: the role of oxygen moieties at graphene surface on gold nucleation and growth. *Chem. Mater*. **2009**, 21, 4796–4802.

(17) Loh, K. P.; Bao, Q. L.; Eda, G.; Chhowalla, M. Graphene oxide as a chemically tunable platform for optical applications. *Nat. Chem.* **2010**, 2, 1015–1024.

(18) Han, Q.; Wang, Z.; Xia, J.; Chen, S; Zhang, X.; Ding, M. Facile and tunable fabrication of Fe_3O_4/graphene oxide nanocomposites and their application in the magnetic solid-phase extraction of polycyclic aromatic hydrocarbons from environmental water samples. *Talanta* **2012**, 101.

388–395.

(19) Wang, X. P.; Lu, J.; Cao, B. Y.; Liu, X. M.; Lin, Z.; Yang, C.; Wu, R. L.; Su, X. T.; Wang, X. F. Facile synthesis of recycling Fe_3O_4/graphene adsorbents with potassium humate for Cr(VI) removal. *Colloid Surface A* **2019**, 560, 384–392.

(20) Bulin, C.; Li, B.; Zhang, Y.; Zhang, B. Removal performance and mechanism of Fe_3O_4/graphene oxide as an efficient and recyclable adsorbent toward aqueous Hg(II). *Res. Chem. Intermediat*. **2020**, 46, 4509–4527.

(21) Yang, X.; Zhang, X.; Ma, Y.; Huang, Y.; Wang, Y.; Chen, Y. Superparamagnetic graphene oxide-Fe_3O_4 nanoparticles hybrid for controlled targeted drug carriers. *J. Mater. Chem.* **2009**, 19, 2710–2714.

(22) Xie, G. Q.; Xi, P. X.; Liu, H. Y.; Chen, F. J.; Huang, L.; Shi, Y. J.; Hou, F. P.; Zeng, Z. Z.; Shao, C. W.; Wang, J. A facile chemical method to produce superparamagnetic graphene oxide-Fe_3O_4 hybrid composite and its application in the removal of dyes from aqueous solution. *J. Mater. Chem.* **2012**, 22, 1033–1039

(23) Grosvenor, A. P.; Kobe, B. A.; Biesinger, M. C.; McIntyre, N. S. Investigation of multiplet splitting of Fe2*p* XPS spectra and bonding in iron compounds. *Surf. Interface Anal*. **2004**, 36, 1564–1574.

(24) Nigam, S.; Barick, K. C.; Bahadur, D. Development of citrate-stabilized Fe_3O_4 nanoparticles: conjugation and release of doxorubicin for therapeutic applications. *J. Magn. Magn. Mater*. **2011**, 323, 237–243.

(25) Wang, J.; Zheng, S.; Shao, Y.; Shao, Y.; Liu, J.; Xu, Z.; Zhu, D. Amino-functionalized Fe_3O_4@SiO_2 core-shell magnetic nanomaterial as a novel adsorbent for aqueous heavy metals removal. *J. Colloid Interf. Sci*. **2010**, 349, 293–299.

(26) Huang, B.; Liu, Y.; Li, B.; Liu, S.; Zeng, G.; Zeng, Z.; Wang, X.; Ning, Q.; Zheng, B.; Yang, C. Effect of Cu(II) ions on the enhancement of tetracycline adsorption by Fe_3O_4@ SiO_2-chitosan/graphene oxide nanocomposite. *Carbohyd. Polym.* **2017**, 157, 576–585.

(27) Li, J.; Zhang, S. W.; Chen, C. L.; Chen, C. L.; Zhao, G. X.; Yang, X.; Li, J. X.; Wang, X. K. Removal of Cu(II) and fulvic acid by graphene oxide nanosheets decorated with Fe_3O_4 nanoparticles. *ACS Appl. Mater. Inter*. **2012**, 4, 4991–5000.

(28) Ma, J.; Wang, W.; Sheng, P. Iron oxide (Fe_3O_4)-graphene oxide (GO) nanocomposites based Li-ion batteries: experimental and theoretical studies. *J. Nanoelectron. Optoe*. **2018**, 13, 1886–1896.

(29) Lu, Q.; Guo, H.; Zhang, Y. Y.; Tang, X. D.; Lei, W. B.; Qi, R. J.; Chu, J. H.; Li, D. Z.; Zhao, Q. B. Graphene oxide-Fe_3O_4 nanocomposite magnetic solid phase extraction followed by UHPLC-MS/MS for highly sensitive determination of eight psychoactive drugs in urine samples. *Talanta* **2020**, 206, 120212.

(30) Zong, M.; Huang, Y.; Zhao, Y.; Zhao, Y.; Sun, X.; Qu, C. H.; Luo, D. D.; Zheng, J. B. Facile preparation, high microwave absorption and microwave absorbing mechanism of RGO-Fe_3O_4 composites. *Rsc Adv*. **2013**, 3, 23638–23648.

(31) Ferrari, A. C.; Meyer, J. C.; Scardaci, V.; Casiraghi, C.; Lazzeri, M.; Mauri, F.; Piscanec, S.; Jiang, D.; Novoselov, K. S.; Roth, S.; Geim, A. K. Raman spectrum of graphene and graphene layers. *Phys. Rev. Lett*. **2006**, 97, 187401.

(32) Liu, Y.; Luo, C.; Cui, G.; Yan, S. Synthesis of manganese dioxide/iron oxide/graphene oxide magnetic nanocomposites for hexavalent chromium removal. *Rsc Adv*. **2015**, 5, 54156–54164.

(33) Zhao, D. L.; Gao, X.; Wu, C. N.; Xie, R.; Feng, S. J.; Chen, C. L. Facile preparation of amino functionalized graphene oxide decorated with Fe_3O_4 nanoparticles for the adsorption of Cr(VI). *Appl. Surf. Sci*. **2016**, 384, 1–9.

(34) Elzinga, E. J. Formation of layered Fe(II)-Al(III)-hydroxides during reaction of Fe(II) with aluminum oxide. *Environ. Sci. Technol*. **2012**, 46, 4894–4901.

(35) Luvsanjamba, M. B.; Sercu, B.; Peteghem, J. V.; Peteghem, J. V.; Langenhove, H. V. Long-term operation of a thermophilic biotrickling filter for removal of dimethyl sulfide. *Chem. Eng. J.* **2008**, 142, 248–255.

(36) Raul, P. K.; Devi, R. R.; Umlong, I. M.; Thakur, A. J.; Banerjee, S. Iron oxide hydroxide nanoflower assisted removal of arsenic from water. *Mater. Res. Bull.* **2014**, 49, 360–368.

(37) Chou, W. L.; Wang, C. T.; Huang, K. Y.; Chang, Y. C.; Shu, C. M. Investigation of indium ions removal from aqueous solutions using spent coffee grounds. *Int. J. Phys. Sci*. **2012**, 7, 2445–2454.

(38) Yang, S. T.; Li, J. X.; Lu, Y.; Chen, Y. X.; Wang, X. K. Sorption of Ni(II) on GMZ bentonite: effects of pH, ionic strength, foreign ions, humic acid and temperature. *Appl. Radiat. Isotopes* **2009**, 67, 1600–1608.